

Packing density of rigid aggregates is independent of scale

Christopher D. Zangmeister^{a,1}, James G. Radney^{a,b}, Lance T. Dockery^a, Jessica T. Young^a, Xiaofei Ma^{a,b}, Rian You^{a,b}, and Michael R. Zachariah^{a,b}

^aMaterial Measurement Laboratory, National Institute of Standards and Technology, Gaithersburg, MD 20899; and ^bDepartment of Chemical and Biomolecular Engineering, University of Maryland, College Park, MD 20742

Edited by David A. Weitz, Harvard University, Cambridge, MA, and approved May 14, 2014 (received for review February 28, 2014)

Large planetary seedlings, comets, microscale pharmaceuticals, and nanoscale soot particles are made from rigid, aggregated subunits that are compacted under low compression into larger structures spanning over 10 orders of magnitude in dimensional space. Here, we demonstrate that the packing density (θ_f) of compacted rigid aggregates is independent of spatial scale for systems under weak compaction. The θ_f of rigid aggregated structures across six orders of magnitude were measured using nanoscale spherical soot aerosol composed of aggregates with ~ 17 -nm monomeric subunits and aggregates made from uniform monomeric 6- μm spherical subunits at the macroscale. We find $\theta_f = 0.36 \pm 0.02$ at both dimensions. These values are remarkably similar to θ_f observed for comet nuclei and measured values of other rigid aggregated systems across a wide variety of spatial and formative conditions. We present a packing model that incorporates the aggregate morphology and show that θ_f is independent of both monomer and aggregate size. These observations suggest that the θ_f of rigid aggregates subject to weak compaction forces is independent of spatial dimension across varied formative conditions.

Many systems are comprised of elementary subunits packed within a defined volume. The simplest 3D system consists of uniform spheres, and despite its apparent simplicity, a rigorous mathematical description eluded researchers for nearly four centuries dating back to Kepler's conjecture in 1611. In 2005, Hales provided a definitive mathematical proof confirming the observed experimental maximum packing density of 74% (1). Packing of more complex structures is far more mathematically challenging and instead relies on empirical studies (2–9). One of the most ubiquitous packing systems in the universe are rigid aggregates composed of a collection of monomeric units joined together into a fractal structure and subsequently densified through omnidirectional applied force, as shown in Fig. 1 (10).

The formation and compaction mechanism of disordered aggregates is presumed to be independent of dimension, composition, and spatial scale, and has been observed in a diverse range of materials and conditions, such as the accretion of material in interstellar space and the formation and compaction of aerosol in the Earth's atmosphere. Many interstellar formations comprise nano- or microscale dust particles that begin as disordered monomeric subunits, which electrostatically aggregate to form fractal (lacey) agglomerates that serve as foundries for comets and planetary seedlings (10–16). Soot, ubiquitous in the Earth's troposphere, is also comprised of nanometer sized carbonaceous monomers aggregated in a disordered lacey structure. Compaction into spheres occurs after trace gas and/or liquid adsorption and evaporation. In both cases, the resulting structure is constrained by aggregate rigidity (17).

The systems described above are similarly constructed from single-unit building blocks assembled into larger disordered structures. The final structure is a function of and emulates the materials and conditions from which it was formed, analogous to structures and networks in biological (allometric scaling), structural, and temporal landscapes that scale over many orders of magnitude (18). Scaling laws govern many relationships, such as vertebrate

body mass and basal metabolic rate with lifetime, fluid flow through hydrological and botanical systems, and complex informational networks (18). In each case, the final structure is defined by the simple power-law expression relating a robust, reproducible subunit to the whole (18):

$$y = C \cdot x^{D_f} \quad [1]$$

where D_f describes the scaling dependence of the system, and C is the scalar quantity over which the system is describing and can possess any unit of measure; i.e., number, length, volume, mass, etc. In scaling systems, D_f is constant over the system domain, and C represents the scale of the unit cell.

This investigation aims to demonstrate that aggregates made from spherical monomers across a broad spatial range form compact assemblies (as shown in Fig. 1) that scale independent of spatial scale (C in Eq. 1) and compaction mechanism and exhibit a constant packing density; this is explored by determining the packing density, θ_f , from the volume occupied by compacted aggregates relative to a total volume (defined as packing density, $\theta_f = V_{\text{agg}}/V_{\text{tot}}$) of nanoscale aggregates made from compact, spherical laboratory generated soot and macroscale aggregates made from 0.60- μm diameter spheres; notably, these structures span six orders of magnitude. For these and other similar systems, we show that θ_f is independent of size.

Compact nanoscale spherical particles were generated from flame generated soot with ~ 17 -nm diameter monomers, (monomer diameter is known as a hereafter) to form lacey aggregates (Fig. 1) with $\theta_f \approx 0.1$, typical for freshly formed soot (19). The particles were compacted by capillary forces into spherically shaped particles by water uptake and evaporation (17, 19). The mass

Significance

Particle aggregates are one of the most ubiquitous structural arrangements in the universe, making up large interstellar planetary seedlings and comets, microscale powdered pharmaceuticals, and nanoscale atmospheric particles. The packing of aggregates determines structure and, in many cases, chemical, physical, and mechanical properties. Here we show that packing in weakly compacted aggregated materials is scale invariant over many orders of magnitude. We demonstrate that the effective density of compacted soot aggregates and comets are equivalent, and conclude that the packing of aggregated materials appear to be remarkably independent of the aggregating forces, mechanisms, or initial conditions.

Author contributions: C.D.Z., J.G.R., and M.R.Z. designed research; C.D.Z., J.G.R., L.T.D., J.T.Y., X.M., and R.Y. performed research; C.D.Z., J.G.R., L.T.D., R.Y., and M.R.Z. analyzed data; and C.D.Z., J.G.R., and M.R.Z. wrote the paper.

The authors declare no conflict of interest.

This article is a PNAS Direct Submission.

¹To whom correspondence should be addressed. E-mail: cdzang@nist.gov.

This article contains supporting information online at www.pnas.org/lookup/suppl/doi:10.1073/pnas.1403768111/-DCSupplemental.

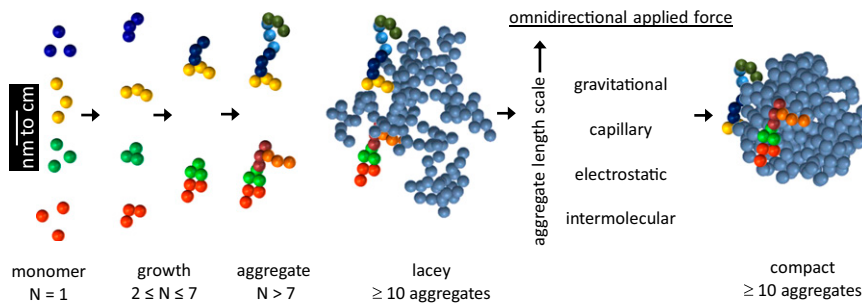


Fig. 1. Size-independent formation of aggregates from spherical monomers into lacey particles and finally to a compact morphology and the forces required for restructuring at each scale.

distributions of the compacted soot as function of particle mobility diameter for an ensemble of particles ($>10^4$ per diameter) were measured. Mobility diameters spanned between 150 and 400 nm in 25- to 50-nm increments (average mass of the compact particles as a function of particle mobility diameter and a representative mass distribution are shown in Fig. S1) (19). Soot particle mass demonstrates a power-law dependence on mobility diameter and is fit well with Eq. 1, where D_f is the mass-mobility scaling exponent relating to the particle shape ($D_f = 1, 2, \text{ and } 3$ for a linear, planar, and spherical particles, respectively). The D_f for compacted soot is 2.96 ± 0.04 (2σ), confirming sphericity, for particles 150–400 nm in diameter, containing 250–4,500 total monomers (N_T), respectively.

Macroscale aggregates were constructed from uniform spherical monomers in random rigid 3D conformations spanning from doublets ($N = 2$) through $N = 12$. The structure of each macroscale aggregate was unique and had a ramified structure, similar to soot aggregates (20). Aggregates with known mass were packed into cylindrical and spherical chambers of known volume, which were large relative to the aggregate dimension (*SI Methods*). Density

relaxation was allowed through gravitational settling by mild tapping (21, 22). Packing density (θ_f) was measured as a function of N .

Packing densities for the nanoscale soot and the macroscale polymer spheres are shown in Fig. 2 along with corresponding transmission electron microscopy (TEM) images and photographs of individual aggregates and their packed forms, respectively (more macroscale aggregates and data of vessel geometry are shown in Figs. S2 and S3). The θ_f of compact soot was determined from the ratio of volume occupied by the monomers ($\rho = 1.8 \text{ g cm}^{-3}$, $a = 17 \pm 2 \text{ nm}$) to the effective volume occupied by the spherical particle as defined by the mobility diameter. For compact soot, the measured θ_f was 0.36 ± 0.02 (2σ) independent of mobility diameter and the total number of monomers (N_T). The packing density of the polymer monomers was determined similarly ($\rho = 1.060 \text{ g/cm}^3$, $a = 6.00 \text{ mm}$). We observe θ_f initially decreases monotonically with N , and for $N \geq 7$ approaches an asymptotic limit of 0.36 ± 0.04 (2σ), consistent with other observations showing θ_f scales as $N^{-1/3}$ (23). Nominally, the final θ_f of a packed system is dependent on experimental protocol (pouring rate, interparticle forces, friction, gravity, frequency, and

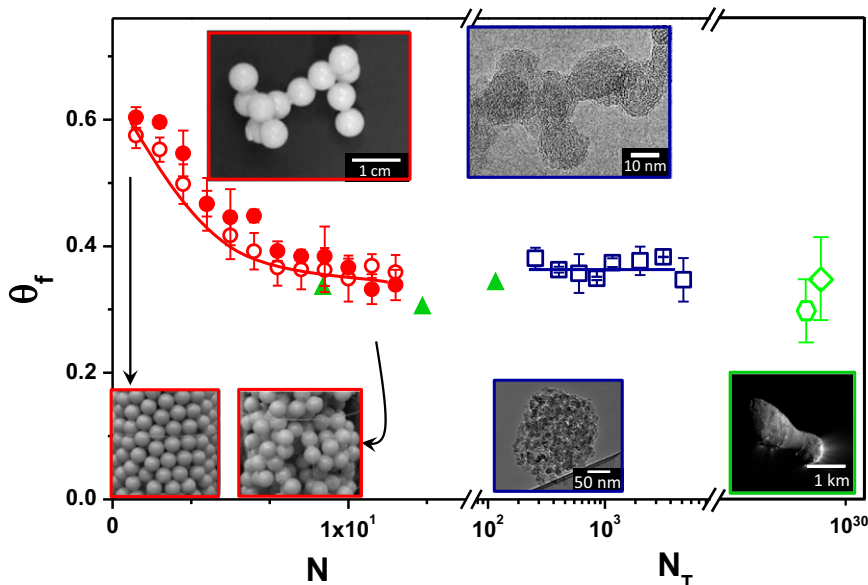


Fig. 2. Packing density (θ_f) as a function of number of monomers with 0.6-cm monomers for $1 \leq N \leq 12$ packed in cylinders (red open circles) and spheres (red filled circles). Red outlined photographs show images of macroscale aggregate with $N = 12$ (Upper) and well-ordered packed volume with $N = 1$ (Left) and highly porous packing with $N = 10$ (Right). Packing density as a function of total number (N_T) of 17-nm monomers in aggregated compact soot (blue open squares). Error bars represent 3σ of 6–10 individual measurements. Green triangles represent calculated θ_f for rigid aggregates as described in ref. 8. Blue outlined photographs show TEM image of aggregated soot (Upper) and 150 nm compacted soot particle (Lower). Calculated packing density for comets 9P/Tempel 1 (green open hexagon) and 103P/Hartley 2 (green open square) using data in refs. 33 and 36. Green outlined image shows image of comet from EPOXI (Extrasolar Planet Observation and Deep Impact Extended Investigation) mission at a range of 696 km. Reprinted with permission from ref. 33.

amplitude of compaction or tapping force) and particle shape (21, 22). In this system, the aggregate structure must also be considered. For any N there exists a distribution of aggregate morphologies defined by the orientation of a monomer or collection of monomers with respect to its neighbors. Using cluster–cluster aggregation theory, studies have successfully modeled both soot aggregate formation and growth into a lacey structure with a D_f consistent with measured values (20, 24, 25). From these investigations, a picture emerges of soot aggregates that have ramified structure similar to the macroscale aggregates used in this study. Given that though similar, the aggregate morphology distributions between the macro and nanoscale likely are not identical. The results indicate that θ_f is independent of both aggregate morphology and scale.

The θ_f of well-ordered close-packed monodisperse spheres is 0.74, and can be as low as 0.49 for ordered tunneled jammed packed assemblies. Measured values are typically ~ 0.64 (random jammed packing), likely setting an upper bound on θ_f for rigid monodisperse aggregates (4, 26, 27). It is important to note that for a jammed system, the transition from random maximum jammed to close packing (for monodisperse spheres, $\theta_f = 0.64 \rightarrow 0.74$) is not possible. As shown here, the packing density of rigid aggregates (0.36 ± 0.04) is much lower than well-ordered spheres and randomly packed nonaggregated spheres, ellipsoids ($\theta_f = 0.74$), cones ($\theta_f = 0.66$), cylinders ($\theta_f = 0.72$), and tetrahedrons ($\theta_f = 0.68$) (7). More remarkably, θ_f is independent of aggregate monomer dimension; i.e., $a =$ nanometers to centimeters. Compared with other packed materials, the θ_f of rigid aggregated monomers are, to our knowledge, among the lowest measured (28). The current results are consistent with simulations of aggregated spherical particles compacted through slight omnidirectional compression ($\theta_f \approx 0.30$ – 0.38 , mimicked in this investigation), and measurements of weakly aggregated micrometer-sized SiO_2 monomers compressed into cakes ($\theta_f = 0.33$) and pharmaceutical powders made from microscale random aggregates ($\theta_f = 0.35 \pm 0.02$) (3, 8, 13). Despite the diverse spatial and formative conditions described above, the θ_f are nearly identical and low compared with θ_f of less rigid systems. It is important to note that the systems described here are under low compression where aggregate morphology is unchanged (i.e., aggregates retain their initial rigid structure without breakage or deformation). Maximum θ_f occurs for rigid aggregates by increasing interdigitation to form a highly entangled final structure. Simulations have shown that increasing the compaction pressure to 100 MPa increases θ_f by $\sim 10\%$ for $N = 9$ and 17 rigid aggregates (8). Thus, 0.39 ± 0.04 likely sets an upper bound on θ_f (8). Increasing interparticle freedom of motion via reduction in aggregate rigidity (degrees of freedom) and hence increased interdigitation, concomitantly increases θ_f , although only slightly. In freely mobile closed looped chains of monodisperse spheres, θ_f is 0.35 for $N \geq 15$ (9). The effect of interaggregate voids on θ_f can be quantified by comparison with rigid, linear rods that show θ_f decreases linearly with increasing aspect ratio (A). Initially, $\theta_f = 0.63$ at $A = 1$ (spherical) and drops to $\theta_f = 0.42$ at an A of 10, which is comparable to the θ_f of rigid aggregates with $N = 5$ – 6 (5). In this investigation, $N \geq 7$ macroscale aggregates, where θ_f is constant, had an A of 1.91 ± 0.19 .

Comets, offer another comparative system, are also comprised of rigid aggregates compacted into a highly porous, fluffy structure, made of mineral dusts, organic materials, amorphous carbon, and ices of CO_2 and H_2O (11). Remote sensing observations of comet 103P/Hartley 2 ($\rho = 0.3 \pm 0.1 \text{ g/cm}^3$) measured $\theta_f \leq 0.3$ (Fig. 2); a similar θ_f was determined for comet 9P/Tempel 1 ($\rho = 0.45 \text{ g/cm}^3$) (29). From a collection of 20 comets, θ_f was calculated to be between 0.2 and 0.4, a range that is remarkably similar to the θ_f measured in this investigation (13). Spectral observations of the ejecta liberated from Tempel 1 after projectile impact (NASA Deep Impact Mission) show the nucleus is constructed of nanometer

to micrometer-sized disordered aggregated fractal (lacey) powders that form a highly porous nucleus in these large-scale aggregates ($N > 7$) using the model shown in Fig. 1 (10, 11, 29). Analysis of captured comet dust grains show they consist of 200- to 500-nm aggregates. Based on analysis of ejected material from comet tails, the aggregates (cometesimals) exist in structures up to several meters in diameter (29–31). The mass density of a range of comet nuclei ($0.15 \text{ g/cm}^3 \leq \rho \leq 0.7 \text{ g/cm}^3$) indicate that the comets described above are typical of other comets in the terrestrial solar system, and that the rigid aggregate packing model can likely be applied to other comets and porous bodies as well (11, 29, 31–33).

The aggregated systems explored here consist of monomers spanning length scales from the nanoscale (soot) through the microscale (comets) and into macroscale, and exhibiting a broad range across N . To understand the dependence of θ_f on monomer and aggregate scale, we investigated the dependence of θ_f on the radius of gyration (R_g), a morphology-dependent parameter that is a function of both aggregate shape (D_f) and size (N). We found that R_g decreases linearly as a function of D_f ranging from 1.5 to 2.25, holding N constant. Representative aggregates at different D_f are shown in Fig. 3A. Aggregates with a $D_f = 1.8$ most closely match those of the macroscale aggregates used in this study, and also capture D_f for experimentally measured aggregated monomers (19, 20). The R_g scales linearly with N for aggregates with $3 \leq N \leq 12$ (Fig. S4) (20, 24, 25, 34). Across the series from individual aggregates to those observed in comet nuclei, the value of N ranged from three per aggregate to 6×10^7 per aggregate, and a spanned from 17 nm for soot to 6 mm for macroscale

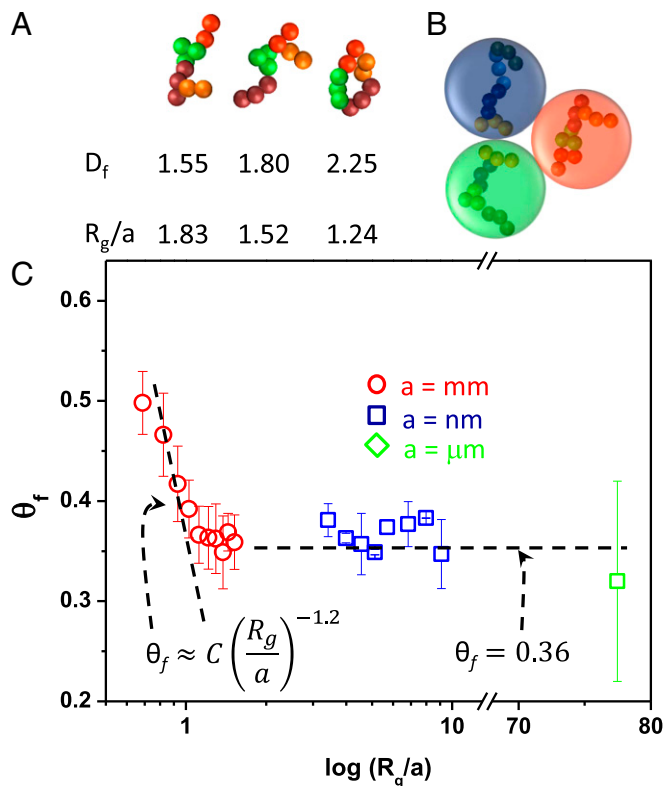


Fig. 3. (A) $N = 10$ aggregates with $D_f = 1.55$, 1.80, and 2.25. (B) Model of $N = 10$ aggregates in the limit of no interdigitation as described in text. (C) Measured θ_f as a function of R_g/a for macroscale rigid aggregates (red open circles), nanoscale soot (blue open squares), and Comet 103P/Hartley 2 (green open square) from ref. 33. Error bars represent 3σ of 6–10 individual measurements and 1σ for macroscale and nanoscale measurements, respectively.

monomers (30). One might expect that given the large range of R_g explored in this study, the commonality observed in the limit of interdigitation must rely in some manner on the relative length scales of a and N . Although a complete theoretical description of the critical length is beyond the scope of this work, we can consider the packing of aggregates under the limiting condition that they do not interdigitate (Fig. 3B). In this limit, the packing fraction is given as the ratio of the absolute volume of the aggregate (V_{agg}) to the spherical volume occupied by the aggregate (V_s), which includes the aggregate and the free space within the aggregate. We can approximate the radius of this occupied volume as R_g .

$$\theta_f = \frac{V_{agg}}{V_s} \propto \frac{(a/2)^3 N}{R_g^3} \quad [2]$$

$$N = k_N \left(\frac{R_g}{a/2} \right)^{D_f}, \quad [3]$$

where a and k_N represents the aggregate diameter and prefactor, respectively (20).

$$\theta_f \propto \left(\frac{R_g}{a} \right)^{D_f - 3} \quad [4]$$

Thus, a natural scaling variable would seem to be the monomer diameter (a), resulting in a dimensionless parameter (R_g/a). In Fig. 3C we show a plot of the measured θ_f as a function of the nondimensional aggregate size for the systems we have explored, which span over an order of magnitude in R_g/a from macroscale aggregates to comet ejecta. We can see that despite the disparate length scales involved, the macroscale and nanoscale overlap and exhibit the same asymptotic hockey stick behavior when normalized by the monomer diameter. The results show that $R_g/a > 1.5$ appears to be a critical limit for interdigitation in aggregate packing, leading to an asymptotic θ_f of ~ 0.36 , where θ_f becomes independent of both a and N for rigid aggregates across the large set of formative conditions described.

This study demonstrates that under low compaction, the packing density, θ_f , is independent of scale for aggregates assembled from spherical monomers spanning the nanometer to centimeter range. The morphology of rigid aggregates is only weakly influenced by monomer shape, suggesting the observations here are not limited to spherical monomers, but can also be applied to aggregates composed of systems constructed of other shapes.

Methods

Soot Aggregate Packing. Soot was generated using a Santoro-style diffusion burner operating on ethylene fuel (19). Freshly generated soot particles were

allowed to aggregate in a 5-L aging chamber for ~ 30 s, forming a lacey fractal morphology. Soot particles were collapsed into a compact spherical morphology through water condensation and subsequent rapid evaporation. Particles were passed through a H_2O growth tube, consisting of a condenser at 10°C and a hydrator at 45°C , and subsequently dried using a tube furnace at 150°C between a pair of SiO_2 diffusion dryers. Size and mass selection were conducted by passing soot through a differential mobility analyzer (DMA) and aerosol particle mass analyzer (APM), respectively, and particles were counted using a condensation particle counter (CPC). The use of a tandem DMA-APM-CPC for measuring particle mass as a function of mobility diameter (D_m) is well detailed (see ref. 19 for a description of the technique). Mass distributions were fit using a Gaussian function over the range where only the (+1) charged particle of interest was present (35). The average mass was used to calculate the mass-mobility scaling exponent (D_f). Packing density was calculated from the measured mass assuming the spherical volume was defined by the particle mobility diameter, a valid assumption for particles with $D_f = 3$. Monomer diameter was measured using TEM of soot aerosol electrostatically deposited on lacey carbon grids.

Macroscale Aggregate Packing. Monodisperse spherical polymer spheres with a diameter of 0.60 μm and a mass of 0.120 ± 0.002 g were combined to form aggregated particles. Particles examined ranged from one-unit monomers through 12-unit (N) aggregates. Monomer units were adhered together in random rigid 3D conformations using a small amount of solvent for dissolution and adherence. Dimers and trimers were initially constructed and added to form larger aggregates. For $N \geq 3$, $\sim 10^3$ aggregates were prepared, and a typical measurement used 30–50% of the aggregates at each N . Aggregate aspect ratio (aggregate length/width) was measured for $4 \leq N \leq 12$ and was 1.88 ± 0.22 . Monomer and aggregate packing was measured in cylindrical and spherical chambers of known volume and varying diameters. To eliminate wall effects, aggregates were measured in containers with radii that spanned several monomer radius units (Fig. S3). Monomer units and assembled aggregates were added to packing chambers and allowed to undergo density relaxation through tapping (defined as lifting by ~ 0.5 cm and dropping the vessel using gravity) and gravitational settling. Particle number concentration and subsequent packing density were determined from the mass of particles within the packing chamber and the volume occupied by the particles. The packing densities of the randomly oriented aggregates were measured for each value of N in triplicate by multiple individuals, with each measurement representing a random and unique population of aggregates. After each measurement aggregates were removed from the vessel and a new, unique aggregate population was measured. Data were averaged for each user and each vessel for all values of N and uncertainties pooled.

Modeling Aggregate Properties. Model aggregates were generated using the cluster–cluster aggregation. D_f was varied from 1.55 to 2.25, a value of 1.6 of k_N was used for all aggregates (24, 25, 34). Aggregates from $N = 3$ –12 were studied.

ACKNOWLEDGMENTS. The authors thank Prof. Salvatore Torquato (Princeton University) for helpful conversations. Funding for this work was provided by a National Institute of Standards and Technology Summer Undergraduate Research Fellowship.

- Hales TC (2005) A proof of the Kepler conjecture. *Ann Math* 162(3):1065–1185.
- Abreu CRA, Tavares FW, Castier M (2003) Influence of particle shape on the packing and on the segregation of spherocylinders via Monte Carlo simulations. *Powder Technol* 134(1-2):167–180.
- Adeyemi MO, Pilpel N (1987) The packing characteristics of physical and formulated mixtures of oxytetracycline and lactose powders. *J Pharm Pharmacol* 39(9):734–735.
- Song C, Wang P, Makse HA (2008) A phase diagram for jammed matter. *Nature* 453(7195):629–632.
- Kyrylyuk AV, Philipse AP (2011) Effect of particle shape on the random packing density of amorphous solids. *Phys Status Solidi A* 208(10):2299–2302.
- Kyrylyuk AV, van de Haar MA, Rossi L, Wouterse A, Philipse AP (2011) Isochoric ideality in jammed random packings of non-spherical granular matter. *Soft Matter* 7(5):1671–1674.
- Li SX, Zhao J, Lu P, Xie Y (2010) Maximum packing densities of basic 3D objects. *Chin Sci Bull* 55(2):114–119.
- Martin CL, Bouvard D, Delette G (2006) Discrete element simulations of the compaction of aggregated ceramic powders. *J Am Ceram Soc* 89(11):3379–3387.
- Zou LN, Cheng X, Rivers ML, Jaeger HM, Nagel SR (2009) The packing of granular polymer chains. *Science* 326(5951):408–410.
- Blum J, Wurm G (2008) The growth mechanisms of macroscopic bodies in protoplanetary disks. *Annu Rev Astron Astrophys* 46:21–56.
- A'Hearn MF (2011) Comets as building blocks. *Annu Rev Astron Astrophys* 49: 281–299.
- Meisner T, Wurm G, Teiser J (2012) Experiments on centimeter-sized dust aggregates and their implications for planetesimal formation. arXiv:1207.3669.
- Blum J, Schrapler R, Davidsson BJR, Trigo-Rodriguez JM (2006) The physics of protoplanetary dust agglomerates. I. Mechanical properties and relations to primitive bodies in the solar system. *Astrophys J* 652(2):1768–1781.
- Blum J, et al. (2000) Growth and form of planetary seedlings: Results from a microgravity aggregation experiment. *Phys Rev Lett* 85(12):2426–2429.
- Dominik C, Tielens A (1997) The physics of dust coagulation and the structure of dust aggregates in space. *Astrophys J* 480(2):647–673.
- Teiser J, Wurm G (2009) Decimetre dust aggregates in protoplanetary discs. *Astron Astrophys* 505(1):351–359.
- Zhang R, et al. (2008) Variability in morphology, hygroscopicity, and optical properties of soot aerosols during atmospheric processing. *Proc Natl Acad Sci USA* 105(30):10291–10296.
- West D, West BJ (2012) On allometry relations. *Int J Mod Phys B*, 10.1142/S0217979212300101.

19. Ma X, Zangmeister CD, Gigault J, Mulholland GW, Zachariah MR (2013) Soot aggregate restructuring during water processing. *J Aerosol Sci* 66:209–219.
20. Sorensen CM (2001) Light scattering by fractal aggregates: A review. *Aerosol Sci Technol* 35(2):648–687.
21. Knight JB, Fandrich CG, Lau CN, Jaeger HM, Nagel SR (1995) Density relaxation in a vibrated granular material. *Phys Rev E Stat Phys Plasmas Fluids Relat Interdiscip Topics* 51(5):3957–3963.
22. McCoy BJ, Madras G (2004) Cluster kinetics of density relaxation in granular materials. *Phys Rev E Stat Nonlin Soft Matter Phys* 70(5 Pt 1):051311.
23. Cumberland DJ, Crawford RJ (1987) *Handbook of Powder Technology* (Elsevier, Amsterdam).
24. Haw MD, Sievwright M, Poon WCK, Pusey PN (1995) Structure and characteristic length scales in cluster–cluster aggregation simulation. *Physica A* 217(3-4):231–260.
25. Jullien R, Botet R, Mors PM (1987) Computer simulations of cluster–cluster aggregation. *Faraday Discuss* 83:125–137.
26. Karayiannis NCh, Foteinopoulou K, Laso M (2009) The structure of random packings of freely jointed chains of tangent hard spheres. *J Chem Phys* 130(16):164908.
27. Torquato S, Jiao Y (2010) Exact constructions of a family of dense periodic packings of tetrahedra. *Phys Rev E Stat Nonlin Soft Matter Phys* 81(4 Pt 1):041310.
28. Hoylman DJ (1970) Densest lattice packing of tetrahedra. *Bull Am Math Soc* 76(1):135.
29. Lisse CM, et al. (2006) Spitzer spectral observations of the deep impact ejecta. *Science* 313(5787):635–640.
30. Kelley MS, et al. (2013) A distribution of large particles in the coma of Comet 103P/Hartley 2. *Icarus* 222(2):634–652.
31. Thomas PC, et al. (2013) Shape, density, and geology of the nucleus of Comet 103P/Hartley 2. *Icarus* 222(2):550–558.
32. Sosa A, Fernandez JA (2009) Cometary masses derived from non-gravitational forces. *Mon Not R Astron Soc* 393(1):192–214.
33. Matrajt G, Flynn G, Brownlee D, Joswiak D, Bajt S (2013) The origin of the 3.4 micron feature in Wild 2 cometary particles and in ultracarbonaceous interplanetary dust particles. arXiv:1301.7470.
34. Liu L, Mishchenko MI, Arnott WP (2008) A study of radiative properties of fractal soot aggregates using the superposition T-matrix method. *J Quant Spectrosc Radiat Transf* 109(15):2656–2663.
35. Radney JG, et al. (2013) Direct measurements of mass-specific optical cross sections of single-component aerosol mixtures. *Anal Chem* 85(17):8319–8325.
36. Lisse CM, et al. (2009) Spitzer Space Telescope observations of the nucleus of Comet 103P/Hartley 2. *Publ Astron Soc Pac* 121(883):968–975.